INSTRUMENTATION

A New Transverse-section Brain Imager for Single-gamma Emitters

Peter H. Jarritt, Peter J. Ell, Melvin J. Myers, Nicholas J. G. Brown, and Judith M. Deacon

The Middlesex Hospital Medical School and Hammersmith Hospital, London, England

Physical and clinical data on a new emission transverse-section scanner are given. Comparative data from an earlier tomoscanner and a rotating gamma-camera system yield the following information for the three imagers.

Resolution at the center of the field is 9 mm for this tomoscanner, 18 mm for the earlier tomoscanner, and 11 mm for the rotating camera; sensitivity (cps/μCi-ml) 36K, 15.4K, 1.9K; crystal area (cm^2) 3096, 619, 490, respectively. The quantification of images is discussed.

Clinical emission section scans of the brain, liver, chest and skull are presented and discussed. Forty brain scans were analyzed in conjunction with x-ray transmission tomography. No false positives were found. From a total of 15 lesions seen by the CT x-ray scanner, 14 were detected by the emission tomographic scanner, 12 by standard gamma-camera imaging. One false negative case (cyst) was seen by the transmission x-ray scanner but not by the emission scanner.

J Nucl Med 20: 319–327, 1979

Although the clinical importance of single-emission transverse tomography has been stressed in work published as early as 1971 (*1*), it seems important to examine the current status of the computer-assisted techniques in relation to recent advances in alternative methods of diagnostic imaging—particularly computerized absorption tomography, (x-ray CT) and imaging with modern gamma cameras. Accordingly, we have evaluated a number of systems being developed for single-gamma emission tomography from the point of view of physical aspects such as sensitivity, resolution, uniformity, and quantitative ability. We have also compared the clinical results obtained with one specific single-emission tomographic imager,* with images of the same patient with conventional gamma camera and x-ray CT techniques.

A number of different systems have been developed for obtaining transverse tomograms with single-emission tracers. These are based on:

1. Multidetector arrays with from two (*2*) to 32 (*3*) individual detectors fitted with long focussing collimators and scanning in a single tangential pass followed by rotation.

2. Multidetector arrays with short-focus collimated individual detectors scanning in a number of tangential passes at different distances from the patient and with no rotation of the assembly.

3. A rotating gamma camera (*4*) with a parallel-hole collimator taking in many planes with one rotatory movement around the patient.

The second of these, the Cleon-710 Transverse-Section Imager, is of recent design and has been installed in our department for assessment of physical characteristics and clinical efficacy. Here in

Received June 19, 1978; revision accepted Nov. 8, 1978.

For reprints contact: Peter Ell, Nuclear Medicine, Middlesex Hospital Medical School, Mortimer St., London W1N 8AA, England.

summary are its main features and mode of operation.

Physical characteristics of the Cleon-710 Imager. The instrument consists of a gantry assembly in which 12 scanning detectors are mounted on radial slide rails arranged in a clockwise fashion at 30° intervals around the opening, which has a diameter of 28.5 cm (Fig. 1). Each detector assembly consists of a focussing collimator (focal length 15 cm), a 20 × 13 × 2.5 cm NaI crystal, light guide, photomultiplier tube (9 cm diam), amplifier, and pulse-height analyzer. These are limited to energies below 300 keV because of the collimator design and the amount of shielding around the photomultiplier tubes. To make the enclosure as compact as possible, the detectors are offset physically and are mechanically coupled so that they do not all move in the same direction at the same time. The motion of the detectors is illustrated in Fig. 1: they move in pairs, such that when one pair of detectors is scanning tangentially and is incremented towards the opening, the adjacent pairs are scanning tangentially and are incremented away from the opening. The focal point of each detector scans half the field of view. Each of the six opposed detector pairs performs a rectilinear scan in the plane of the slice over the brain from a different angle. The detectors perform 12 tangential line scans spaced at 1 cm, each line being 20 cm long (the effective diameter of the field of view) and divided into 128 resolution elements.

The output from each detector is sampled in rotation every 4.8 μsec. If in any detector an event is detected, it is transferred by the data bus to accumulators, where the sampling and accumulation process continues until one resolution element has been transversed. The data in the accumulators are then transferred via a direct memory access (DMA) link into the computer† memory, where they are stored until a complete slice has been scanned. The reconstruction of each individual image takes 2 min.

Initially, each scan is dynamically corrected for nonuniformity of detector response. Since each detector scans the central region of the field, the counts recorded by each detector from this area are compared. Opposing detectors are initially normalized to each other and then the sums obtained from the six detector pairs are compared to give 12 normalization factors for the detector array. A fixed but small correction for photon attenuation (less than 5% at center of image) is applied.

The reconstruction algorithm uses a modified Radon filter, which was first solved by Radon in 1917 (*5*) and its use has recently been outlined by

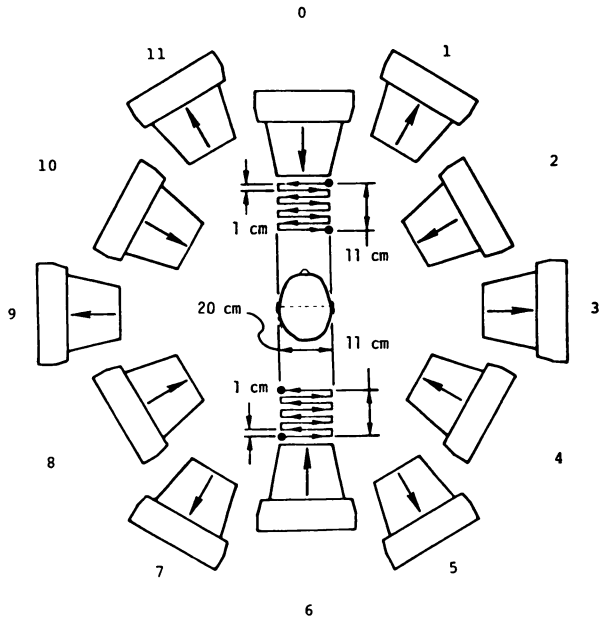

FIG. 1. Diagram to show detector motions for six opposing pairs of the Cleon-710.

Cormack (*6*). The input data consist of six rectilinear scans over the field of view, offset from each other by 30°. A composite array can then be formed by the superposition of these six scans giving a distribution approximately circularly symmetric. Each data point will consist of counts that originated from the collimator focus while scanning that point, together with contributions from off-focus radiation, the proportion depending on the collimator's changes of sensitivity with depth.

Radon's result states:

For any point Q in a plane, take the average of the line integrals of lines that are tangent to a circle of radius p with Q as its center. That is, form

$$\bar{f}(p) = \frac{1}{2\pi}\int_0^{2\pi} f(p), \phi) d\phi, \qquad (1)$$

where $f(p,\phi)$ is a line integral defined with Q as the origin of the polar coordinates (p,ϕ). Then the value of g at the point Q, g(Q) is

$$g(Q) = -\frac{1}{\pi}\int_0^{\infty} \frac{d\bar{f}(p)}{p} = -\frac{1}{\pi}\int_{\pi}^{\infty} \frac{d\bar{f}}{dp}\cdot\frac{dp}{p}. \qquad (2)$$

Thus, the value of g at Q can be found simply if the detector system is designed to measure $f(p,\phi)$ at points that are a distance p from Q. The sum of such points gives $\bar{f}(p)$. If values can be obtained for a number of values of p, the integration in Eq. 2 can be carried out. By a change of the coordinate origin, this integration can be obtained for all points in the plane. The composite array described above

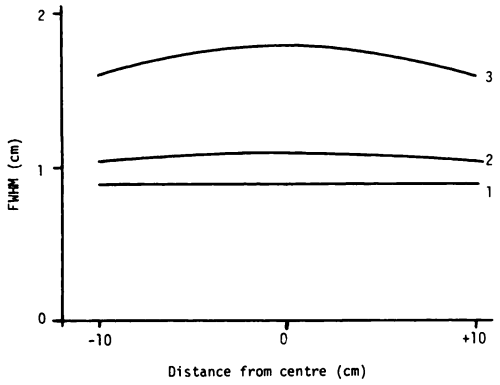

FIG. 2. Comparative data for resolutions of three single-photon tomographic imagers. (1) Cleon-710 (2) Budinger *et al.*(4) (3) Kuhl *et al.* (3).

provides $f(p,\phi)$ throughout the plane, but the values are modified by the off-axis radiation and the integration in Eq. 2 is modified by a filter of the form $1/p^{\chi}$, where $1 < \chi < 2$.

When operated in automatic mode, the instrument is capable of collecting up to eight slices with simulataneous reconstruction and display, thus minimizing a patient's study time. The spacing between slices can be selected in multiples of 3 mm and is automatically controlled by the patient's couch movement. The gantry can be tilted through an angle of ±20° to the vertical to allow the selection of image sections at various appropriate angles.

The operator's console is used to control the process of scanning, data acquisition, reconstruction, and display. Reconstructed data are displayed as two adjacent images, each of 128 × 128 elements. These are derived independently from the input data, using two filtering coefficients, one producing a more smoothed image. Interaction with the images to control background subtraction, saturation, and gray-scale assignment is facilitated through thumb switches mounted on the console. Hard-copy outputs are available on transparent and/or Polaroid film.

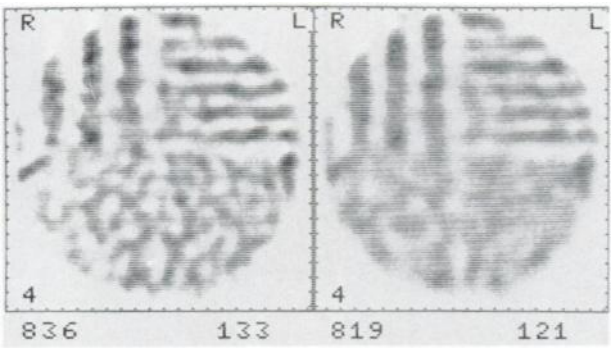

FIG. 3. Results obtained from the Cleon-710 imager for reconstruction of 3-D bar phantom containing 250 μCi of Tc-99m. Resolved plates are spaced at 13 mm and 9 mm.

METHODS AND RESULTS

We have measured the following physical parameters, which determine the imaging capabilities of the instrument:

1. resolutions in the two displayed images;
2. thickness of the slice as measured by the full width at half maximum of the slice ($FWHM_{sl}$);
3. sensitivity of the detector assembly; and
4. quantification of count-rate response.

The measurement of the Line Spread Function (LSF) within a slice. The LSF for Tc-99m was measured using a phantom consisting of a circular plexiglass block, 20 cm in diameter and 5 cm thick, in which a series of 2.5-mm holes had been drilled in a spiral pattern. These allowed the measurement of the LSF at different depths within the scattering material. A short length of polyethylene tubing containing a solution of Tc-99m (10 mCi/ml) was inserted into each hole in turn and 2-min scan performed. The results are shown in Fig. 2. These were obtained by using profiles through the point source and calculating the FWHM as a function of resolution elements. The results indicate that the FWHM is 9 mm in the high-resolution reconstruction and that in the lower-resolution reconstruction FWHM = 11.5 mm. These values do not vary with depth of scatter and are constant over the entire field of view.

There are artifacts in the reconstructed image, caused not by detector inhomogeneity or movement, but by the algorithm and the sampling limitations. These manifest themselves most clearly with a point source where the reconstructed object is surrounded by a 12-pointed star radiating from the object. These are present at every point in a reconstructed image, and to confirm the values obtained for the line source response, a phantom was constructed consisting of a hollow perspex cyclinder, 20 cm in diameter by 5 cm deep, with a wall thickness of 5 mm. Mounted in each quadrant was a set of perspex plates. Each set had a different thickness, the spacing being equal to this thickness. The values chosen were 13, 9, 5, and 3 mm. A reconstruction of this complex phantom was obtained using concentrations of activity typically found in brain scanning with a comparable scanning time. The results for a phantom containing 250 μCi are shown in Fig. 3. The plates spaced at 13 mm and 9 mm can be clearly seen. The effect of the reconstruction artifact is to produce a uniform

background activity without degrading the resolution of the instrument. The magnitude of this contribution varies between the two reconstructed images but corresponds to 20–25% of the peak activity level.

Measurement of slice width ($FWHM_{sl}$). The thickness of the section viewed by each of the three instruments was determined from the resolution of the collimator (not being subject to degradation by the reconstruction process) and was measured from the conventional line source response in a direction perpendicular to the plane of the slice for the rotating camera and the conventional tomoscanner. In the Cleon, the response is summed over a number of distances along the collimator axis, so that the thickness could be measured only by reconstructing the image of a source and moving the source along the axis perpendicular to the plane. A uniform source thickness of 15 mm was found. This may be compared with the convex disc-shaped sensitive volume formed by the spreading-out collimator response of the camera device rotated around the plane, and with the concave disc-shaped sensitive volume formed by the conventional long-focussed device, whose response is designed to narrow near the center of the section. The results for section thickness are shown in Table 1.

Measurement of sensitivity. The sensitivity of the instrument was measured by the method of Kuhl et al. (*3*) using a cylindrical source 20 cm in diamter and 20 cm long, filled with a known amount of Tc-99m. The results for the three devices are summarized in Table 2. Included in the table are the total areas of detecting crystal for each instrument, thus indicating how the basic sensitivity has to be sacrificed to achieve better resolution (see the comparison of resolution data, Fig. 2).

Quantification. The ability of tomographic imaging devices to produce quantitative images has long been recognized. However, absorption correction, motion, and algorithm artifacts have limited their usefulness. The shape of the sensitive volume created is also important from the point of view of quantifying the data. Since the results are to be expressed as μCi/ml, the shape of the volume element (boxel) must be known. If this is a function of position in the reconstructed plane, a further inaccuracy in concentration measurements may be introduced.

An initial assessment of the ability of the Cleon-710 imager to produce quantitative images was undertaken using a 1-cm^3 source placed within a block of plexiglass. Known amounts of Tc-99m activity were placed in the source and scanned using a 4-min slice time. The results are shown in Fig. 4,

TABLE 1. SLICE THICKNESS VALUES FOR THREE SINGLE-PHOTON EMISSION DEVICES ($FWHM_{sl}$)

Device	Center	10 cm from Center
Cleon-710	15 mm	15 mm
Kuhl Mk IV*	17 mm	20 mm
Gamma camera†	Selectable biconvex disc	

* Kuhl et al. (*3*)
† Budinger et al. (*4*)

TABLE 2. RELATIVE SENSITIVITIES FOR THREE SINGLE-PHOTON EMISSION TOMOGRAPHIC IMAGERS

Device	Sensitivity (cps/μCi-ml)	Area of crystal detector (cm^2)
Cleon-710	3600	3096
Kuhl Mk IV*	15,400	619
Gamma camera†	1900	490

* Kuhl et al. (*3*)
† Derived from Budinger et al. (*4*)

where the peak count in the image has been plotted against the number of μCi in the phantom. These results suggest that very accurate quantification is possible. However, when a single uniform source is used, the reconstruction artifacts can be ignored, since one can select a region of interest that eliminates this contribution. Where a more complex phantom is used (consisting of an array of 39 cells, 18 × 18 mm, containing known, differing amounts of activity) it is possible to achieve the same accuracy in quantification. However, the data must be modified by subtracting 25% of the peak activity level, which removes the background caused by the

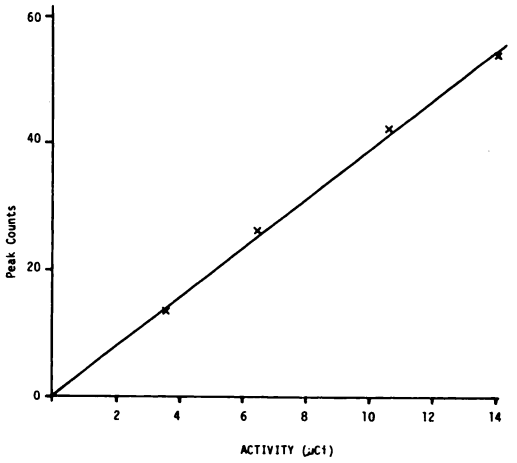

FIG. 4. Quantification of source activity using Cleon-710 imager. Single volume source imaged with 4-min slice time.

reconstruction artifacts. Although the calibration has been expressed in terms of peak counts, comparable results are obtained using total counts within a region of interest. It must necessarily be assumed that the activity distribution extends uniformly through the slice in order to express the results as μCi/ml, but with the above restriction, variation of the size and shape of the object does not affect the quantitative accuracy. Note, however, that a single source of very much greater activity than the remainder of the field will result in inaccuracies caused by a predominant reconstruction algorithm centered at this point. Our results with the 39-cell phantom correspond with those of the MkIV system of Kuhl (*3*), who has shown that by taking the central areas of activity (4 cm^2) from an array of 3- by 3-cm sources, a correlation of 0.99 can be achieved between the activity calculated from the scan and that in the phantom.

It is instructive to place a uniform source within a tomographic system in order to test for a) the noise patterns expected in normal levels of activities, b) the effects of any attenuation corrections in the reconstruction program, and c) to show up any artifacts inherent in the mode of acquiring data. For example, the camera system is prone to circular artifacts of seemingly high activity distributed in rings in the section. These can result from two independent origins: a) the incorrect assignment of the center of rotation; and b) the rotation of areas of increased sensitivity around a true center of rotation. It is thus essential that sensitivity inhomogeneities be kept below 3% by uniformity correction of data and that rotation-center errors be below 5 mm. Our results have shown that the system described is capable of obtaining high-resolution images. The detector system is not prone to acquisition artifacts and requires only a very small attenuation correction. The reconstruction of a slice of uniform thickness has enabled accurate quantitative data to be obtained.

CLINICAL APPLICATIONS

With conventional projections, the contributions from neighboring structures are superimposed on the feature of interest. A section image, on the other hand, allows the separation of a feature of interest within an organ from neighboring structures. This simple consequence of the tomographic approach to imaging explains the wide acceptance and success that computerized tomographic procedures enjoy today. If imaging technology allows enough structural detail to be displayed (as in computerized tomographic x-ray systems), the clinical advantages are immediately apparent. However, for a more informed approach to diagnosis, additional information is required. This includes information concerning function, metabolic activity, blood supply (flow and volume), and changes in these parameters with time, drug therapy, or active surgery. This entirely new approach in the evaluation of organ disease (with emphasis on biochemical and functional characterization rather than on structural change) is the foundation for new emission tomographic systems.

As part of the initial evaluation of this tomographic scanner, over 60 patients were investigated using standard Tc-99m-labeled pharmaceuticals. The scanner was operated with Tc-99m window settings, covering 130–170 keV, a scan time of 4 min per slice, and a slice spacing of 1.25 cm. In the case of brain imaging with pertechnetate, a background cut-off of 25% was chosen, since this gave the best clinical display. All images were displayed on transparent film with 16 levels of gray. Since the machine has been designed as a head scanner, the majority of the investigations concern the brain and skull. However, a few clinical examples of chest and liver sections were obtained. Figure 5 shows a transverse section of the chest of a 7-year-old boy referred for evaluation of an osteosarcoma of the left femur. Fifteen mCi of Tc-99m MDP were given intravenously, and the section scan was made 90 min later. The outline of the rib cage, the vertebral body, spinal processes, and spinal canal are seen with excellent definition. The detail and information available raise hope for future investigation of diseases involving the spinal canal with this technique.

Figure 6 shows a transverse section of the head of a 42-year-old woman with known lytic bony lesions in the pelvis and left femur. The skull radiograph shows a large metastatic lesion in the par-

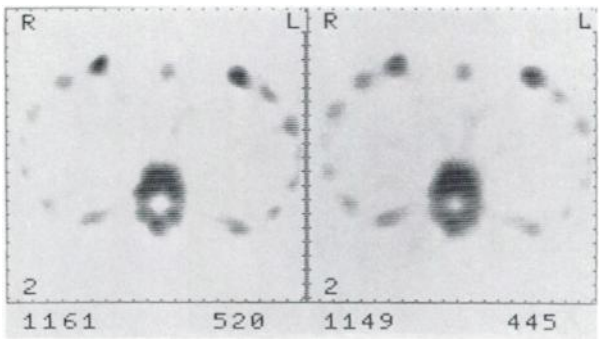

FIG. 5. Emission section scan of the chest of 7-year-old male patient with 15 mCi of Tc-99m MDP. Scan done 90 min after injection. Slice time = 4 min. Note considerable detail in image, with clear resolution of spinal canal.

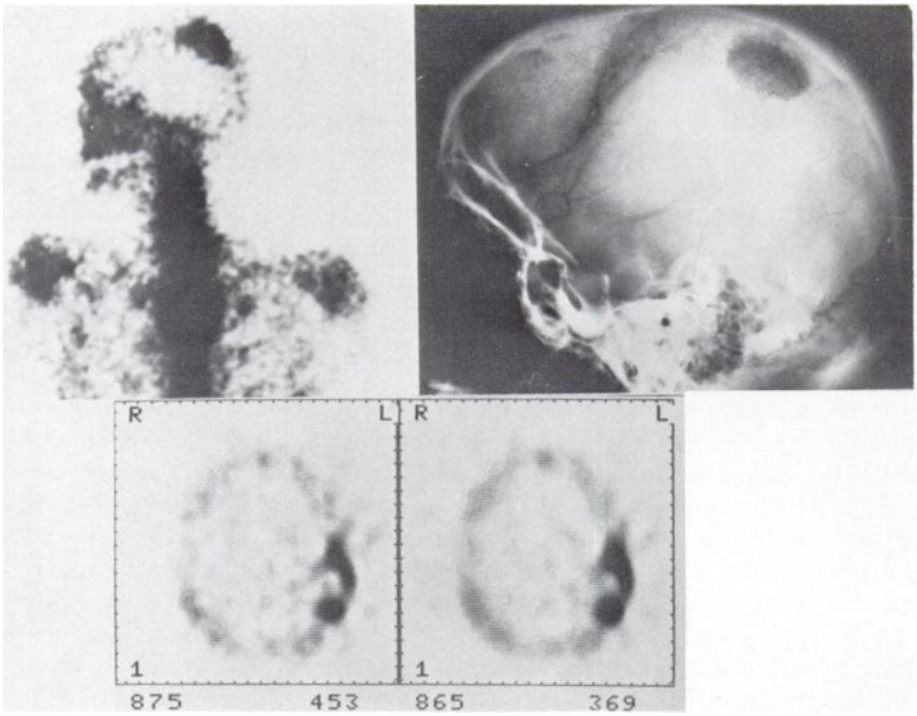

FIG. 6. Female patient, 42 years old, with lytic bony lesions in pelvis and femur. Skull radiograph, bone scan, and emission tomography. Metabolically active lesions best displayed by emission section scanner.

ietal bone. The metabolic activity of this area is seen and confirmed in the gamma-camera radionuclide skull scan but is best imaged with the section scan, where two lesions with intense uptake are well demonstrated.

Figure 7 shows a series of transverse-section scans of the abdomen of a 5-year-old child with Hodgkin's disease and hepatosplenomegaly. The tomographic display shows the liver and spleen in their normal positions (note *R* and *L* markings). Detailed anatomy of the liver can be seen, with the porta hepatis and liver lobes displayed. The spleen is in the normal location.

Figure 8 is from a patient with a primary brain tumor in the cerebello-pontine angle, well displayed on the gamma-camera image and clearly seen in relation to neighboring structures, both with the emission scanner and the x-ray transmission scanner. Note the degree of functional detail present on the emission image, which is such that it begins to resemble the transmission "electron density" image.

Figure 9 shows images from a 50-year-old woman with carcinoma of the breast, who presented after a recent epileptic fit. The gamma-camera image reveals a single area of increased tracer concentration in the left frontal lobe. The sections obtained with the emission scanner show two areas of abnormal tracer concentration, one corresponding to the left frontal lesion. A suspected diagnosis of a single cerebral metastasis can be altered to a definite diagnosis of multiple secondaries.

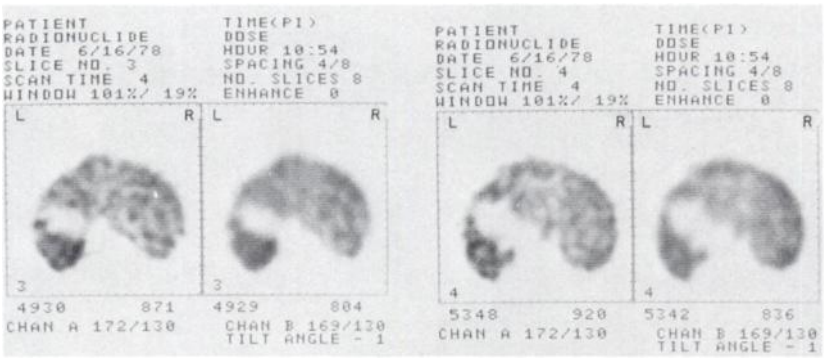

FIG. 7. Emission section scans of abdomen of 5-year-old child with Hodgkin's lymphoma and hepatosplenomegaly. Note 'L' and 'R' signs. Tc-99m sulfur colloid, 500 μCi. Right and left lobes and porta hepatis well displayed, as is spleen shadow.

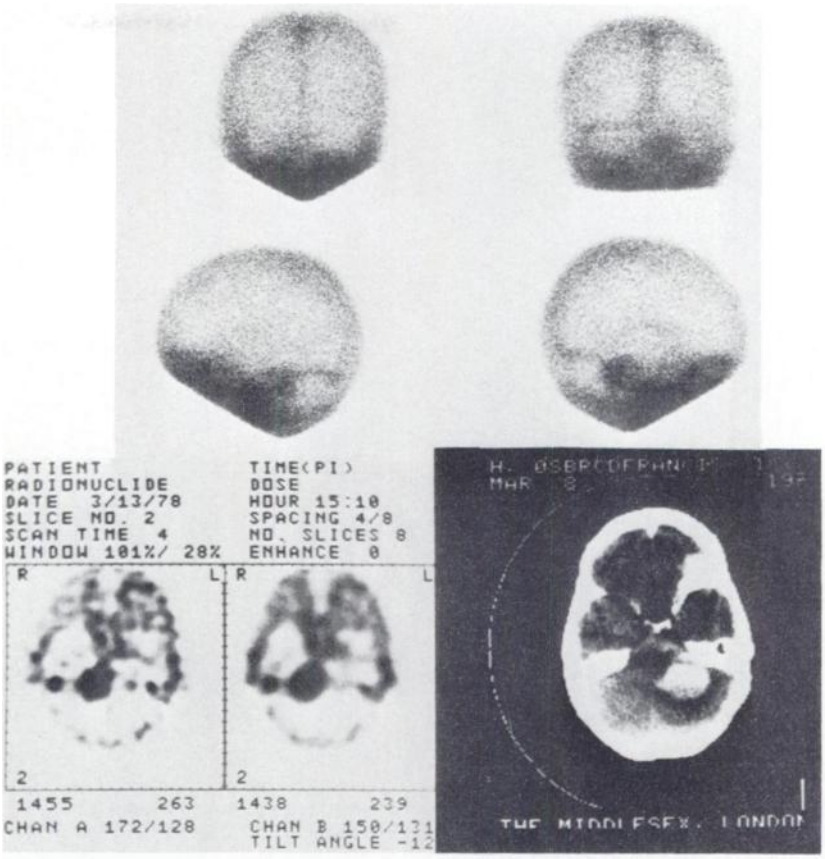

FIG. 8. Tumor of cerebello-pontine angle. Comparisons between analog brain scan, EMI transmission scan, and emission tomoscans of head (Tc-99m). Note degree of functional detail in emission section scans, with sections showing clear detail in anterior, middle and posterior fossae.

Forty brain scans were analyzed in conjunction with x-ray transmission tomography. No false positives were found. From a total of 15 lesions seen with the CT x-ray scanner, 14 were detected by the emission tomographic scanner and 12 by standard gamma-camera imaging. One false-negative case (cyst) was seen by the transmission x-ray scanner but not by the emission scanner.

DISCUSSION

It is clear that emission tomography is opening new areas of research, both in the domain of instrument development and in the area of clinical applications. To some extent, the functional mapping of sections of organs is still waiting, not only for new radiopharmaceuticals but also for clinical problems that require this approach for their solution. Nevertheless, present technology is indicating some possible uses for these machines. The high sensitivity of detection of space-occupying disease in the brain—obtained at one-twentieth of the radiation dose delivered to patients scanned with x-ray transmission techniques‡—underlines the potential screening role of the emission approach. This by itself may play an important role in those neurologic centers where an excessive input of patients for x-ray transmission imaging has caused undesirable clinical and logistic problems. A strategy for the use of emission and transmission techniques will need to be implemented if these imaging methods are to be used to the best advantage. In other words, a finer selection of patient material for CT input is required (*8*). Not every cerebrovascular accident or cerebral tumor may need a CT scan, and sufficient clinical information may be obtained from an emission brain scan. Assuming that time per test is similar (total time for an emission brain scan in this study is 35 min), the benefit of CT scanning can be enlarged (by reducing waiting lists) with proper selection of patients.

Much of the success of emission tomography will be linked to the development of new radiopharmaceuticals and short-lived emitters. If cyclotrons become practical within a hospital environment, in terms of their physical size and cost, the availability of the aforementioned radiopharmaceuticals will expand. On the other hand, it is possible that generator-based short-lived radionuclides will also play a role (Br-77→Se-77, Ge-68→Ga-68, etc.). In any case, greater problems may arise with the progressive need for very fast radiolabeling techniques and quality-control protocols (sterility and pyrogenicity, for example, are relevant aspects to bear in mind). On the other hand, the goal of in vivo and

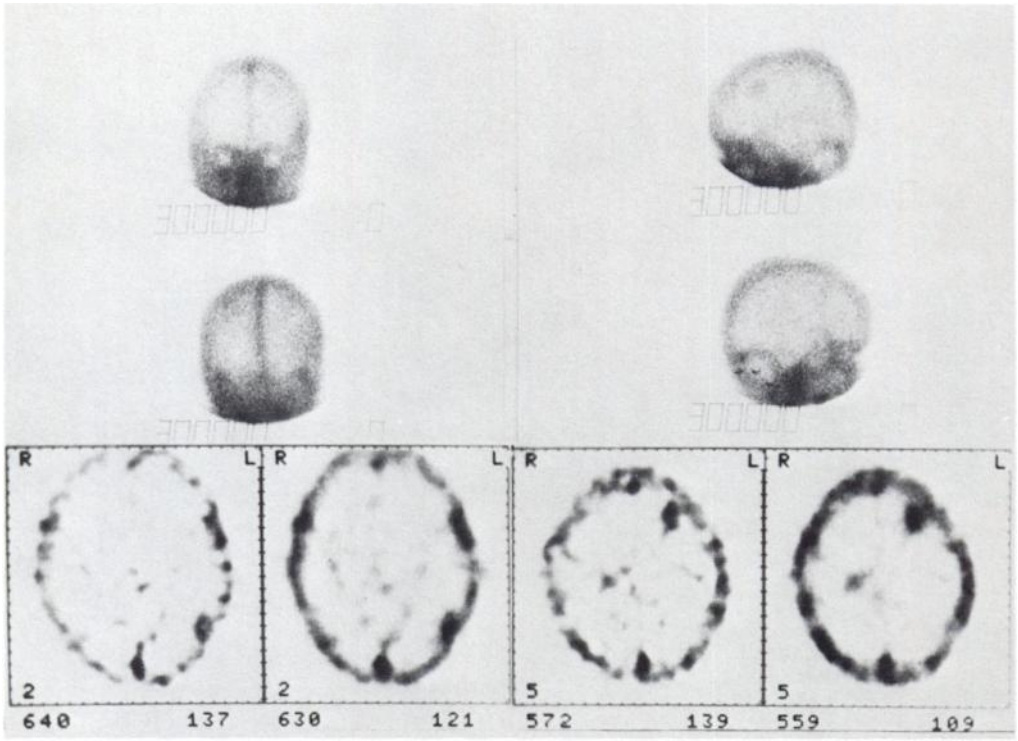

FIG. 9. Cerebral metastases from breast carcinoma. With conventional gamma cammera (above) only a single shadow (left frontal) is seen. Further deposits (left frontal and right temporal) are shown by emission section scans. Other imaging abandoned because clinically irrelevant.

functional "autoradiography" may not be so far away, considering progress in the available radiopharmaceuticals—iodine-labeled monoclonal antibodies, diffusible indicators such as antipyrine, lipid membranes delivering the enclosed radionuclide to a target organ, metabolic substrates such as dopamine or glucose analogues, enzyme inhibitors, etc.

There are fundamental differences between the three approaches to single-photon detection discussed. However, there remain several common requirements: a) uniform resolution and sensitivity with depth; b) accurate correction for photon attenuation; and c) uniform detector response to activity concentration, allowing accurate quantification. It has been argued (*9*) that the use of a rotating camera will result in lower instrument cost, together with the advantageous ability to record multiple slices at the same time. However, a device optimized for the imaging of two-dimensional projections (i.e., camera-like devices), rather than for specific single-slice transaxial imaging, is at a disadvantage from the point of view of imaging time. The potential for providing conventional two-dimensional projection images is possessed by all devices, although rotating gamma cameras, owing to their large field of view, will have the advantage of ease of reconstruction in planes other than that normal to the axis of rotation. Their use in longitudinal reconstructions is therefore quite common (*10*).

The scanning systems may offer a more artifact-free reconstructed image because of the inherently more uniform method of data acquisition. Whichever system is used, it must be capable of sectioning an organ to give a map of *quantitative* tracer concentration with high resolution and accuracy. The removal of superimposed information in this imaging technique allows the measurement of aspects of physiologic function not possible in the past.

FOOTNOTES

*Union Carbide Cleon-710, Rye, NY

†Data General S/230 Eclipse

‡Assumes that the standard dose from a brain scan with Tc-99m is in the order of 100 mrad and that the dose to a slice in the brain from transmission scans can vary between 1.5 to 2 R (*7*).

REFERENCES

1. KUHL DE, SANDERS TP: Characterizing brain lesions with use of transverse section scanning. *Radiology* 98: 317-328, 1971

2. BOWLEY AR, TAYLOR CG, CAUSER DA, et al: A radioisotope scanner for rectilinear, arc, transverse section and longitudinal section scanning: (ASS—the Aberdeen Section Scanner) *Br. J. Radiol.* 46: 262-271, 1973

3. KUHL DE, EDWARDS RQ, RICCI AR, et al: The Mark IV system for radionuclide computed tomography of the brain. *Radiology* 121: 405-413, 1976
4. BUDINGER TF, DERENZO SE, GULLBERG GT, et al: Emission computer assisted tomography with single-photon and positron annihilation photon emitters. *J Computer Assisted Tomography*. 1: 131-145, 1977
5. RADON J: Über die Bestimmung von Funktionen durch ihre integralwerte längs gewisser Mannigfaltigkeiten. *Ber Verh Sachs Akad Wiss* 67: 262-271, 1917
6. CORMACK AM: Reconstruction of densities from their projections, with applications in radiological physics. *Phys Med Biol* 18: 195-207, 1973
7. MCCULLOUGH EC, PAYNE JT, BAKER HL, JR, et al: Performance evaluation and quality assurance of computer tomography scanners, with illustrations from the EMI, ACTA and Delta scanners. *Radiology* 120: 173-188, 1976
8. ELL PJ, TODD-POKROPEK A, WILLIAMS ES: The future of non-invasive medical imaging. *Röfo* 128: 486-490, 1978
9. KEYES JW, ORLANDEA N, HEETDERKS WJ, et al: The Humongotron—a scintillation camera transaxial tomograph. *J Nucl Med* 18: 381-387, 1977
10. MUEHLLEHNER G, ATKINS F, HARPER PV: Positron camera with longitudinal and transverse tomographic capabilities. In *Medical Radionuclide Imaging 1976*, Vol. 1, Los Angeles, IAEA, 1977, 291-307